RESEARCH ON SAR IMAGE TARGET RECOGNITION ALGORITHM BASED ON NSCT+PNN

Dong LI[1,*], Binwen GAO[2], Ye LI[3]

Based on Synthesis Aperture Radar (SAR) image preprocessing, this paper proposes a SAR image target recognition method based on non-subsampled Contourlet Transform (NSCT) for feature extraction and Probabilistic Neural Network (PNN) for target recognition. On the basis of studying the denoising of multi-scale geometric analysis theory, the low-frequency components and high-frequency components of SAR image samples are extracted by NSCT respectively. The target eigenvectors are obtained by PNN. This method was used to extract and identify the three types of military targets in the MSTAR database. The recognition rate was 90.7%. The results show that the SNCT+PNN method can effectively achieve SAR target recognition and obtain a higher target correct recognition rate.

Keywords: SAR, NSCT, PNN, Feature extraction, Target recognition

1. Introduction

With the rapid development of radar signal processing technology, Synthetic Aperture Radar hereinafter referred to as (SAR) has been further developed with all-weather, long-range and large-scale detection performance. The study of extraction of target texture and edge features and target recognition algorithm plays a key role in the popularization and application of SAR [1]. In this paper, SAR image preprocessing, feature extraction and target recognition are studied. In the SAR image preprocessing part, aiming at the SAR imaging mechanism and the principle of speckle noise generation, the enhanced Lee filtering [2], wavelet soft threshold filtering (WT-soft) [3], Curvelet hard threshold filtering [4], Ridgelet transform and Contourlet + PCA [5] filtering denoising method are compared and analyzed, and the advantages and disadvantages of the algorithm are evaluated quantitatively by ENL, EPI and other parameters. The multi-scale decomposition method NSCT based on Contourlet transform is used to decompose the low frequency components including the image contour information and the high-frequency components including the edge and detail information of the image. LBP and HOD operators are used to construct

[1] Lect., College of information engineering, Inner Mongolia University of Technology, China
[2] Eng., Inner Mongolia power, China
[3] Lect., Hohhot Vocational Collage, China
* Corresponding author: Dong Li, email: 15949411984@163.com

the SAR image classification vectors respectively. The normalized feature vectors are classified and identified by PNN. The feature extraction and recognition experiments are carried out for four kinds of military targets in Moving and stationary Target Acquisition and Recognition (MSTAR) database. It is supported by multiple ground targets of the U.S. Defense Agency. The recognition rate is 90.7%, and the correct target recognition rate is high, which validates the effectiveness of the method.

2. SAR Image Preprocessing

2.1 Research on typical filtering algorithm

In practical engineering applications, the SAR image is heavily correlated with speckle noise from the SAR imaging mechanism [6]. The necessary preprocessing must be done before image target recognition. Reducing the speckle noise of SAR images usually includes: airspace method, transform domain method and other methods. In this paper, several filtering methods mentioned are compared and analyzed. Among them, enhanced Lee filtering is a typical spatial filtering method, WT soft, curvelet hard threshold filtering and ridgelet transform are typical filtering methods in transform domain, contourlet + PCA filtering is a filtering algorithm combining transform domain and statistical methods. The number of HB15270 in the MSTAR database 2S1-b01 is selected as the object of denoising, as shown in Fig. 1.

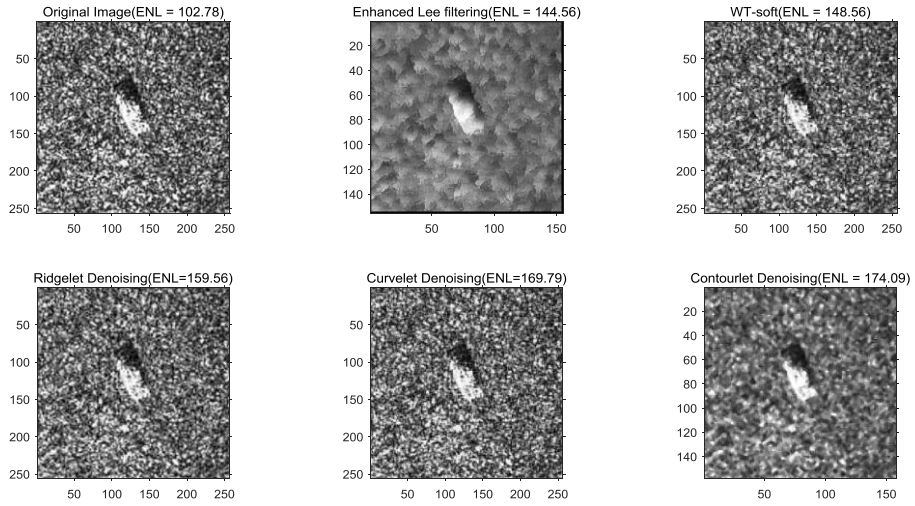

Fig. 1. HB15270 Denoising simulation image

2.2 SAR image quality assessment

After filtering the SAR image, it is impossible to quantify the image quality of preprocessing filter results because of the unknown parameters of SAR

ideal image, the Signal noise ratio (SNR) and other evaluation parameters that require the priori information of images. In this paper, the equivalent visual number (ENL) and edge holding index (EPI) are introduced, which takes three parameters of t-csg time. ENL is the square ratio of mean and variance, and the ratio is high. It shows that the ability of denoising is relatively strong, otherwise the noise reduction ability is relatively weak [7].

$$ENL = \frac{\mu^2}{\delta^2} \tag{1}$$

The edge preserving index (EPI), as shown in formula (2), is shown as follows: A is the image before denoising, and B is the image after denoising. If the ratio of the equation is large, it shows that the noise reduction effect of the algorithm is better, and the range of EPI is (0,1).[8]

$$EPI = \frac{\sum\left(\left|B(i,j)-B(i+1,j)\right|+\left|B(i,j)-B(i,j+1)\right|\right)}{\sum\left(\left|A(i,j)-I(i+1,j)\right|+\left|A(i,j)-A(i,j+1)\right|\right)} \tag{2}$$

The number of HB15270 in the MSTAR database 2S1-b01 is selected as the object of denoising, and the parameters data as shown in Table 1 are calculated. From this we can see that single spatial domain or transform domain methods such as Lee filtering, wavelet filtering, Ridgelet filtering and so on. Although the computation time is small and the time is small, the effect is not obvious. Ridgelet transform, curvelet transform and contourlet transform solve the defects of finite directivity and isotropy of wavelet transform, and retain most of the high-dimensional singular information such as edge and contour of the image, a lot of scratches and embedded stains are added to the image. There is spectral aliasing problem. In view of the above problems, this paper combines transform domain method with statistical class method, that is, denoising SAR images with Contourlet + PCA filtering denoising method. From the view of equivalent number and edge preserving index, the filtering effect of this method has been improved.

Table 1

HB15270 simulation results

Image characteristics	ENL	EPI	Time consuming
Original image	102.78	/	/
Enhanced Lee filtering	144.56	0.514	0.347
WT-soft	148.56	0.533	0.386
Ridgelet	159.56	0.632	0.453
CT-hard	169.79	0.644	0.478
Contourlet+PCA	174.09	0.694	0.578

3. Feature Extraction based on NSCT

In 2006, aiming at the serious aliasing phenomenon in the frequency domain direction of the detail signal in the Contourlet transform, Cunha put forward a completely translation invariant non-Sampling Contourlet transform (NSCT) [9-11]. NSCT uses the stationary wavelet transform and the upper interpolation directional filter similar to the pyramid algorithm [12] instead of the Laplace transform and the directional filter of the original Contourlet transform. In this way, the frequency aliasing phenomenon of the original directional filter is greatly reduced. By means of NSCT decomposition, the low-frequency components containing image contour information and different levels of high-frequency components with edge and detail information can be obtained. As shown in Fig. 2, the results of NSCT decomposition of zoneplate images are given.

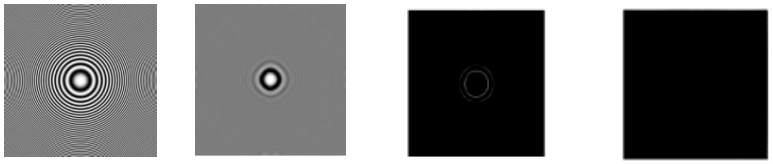

(a) Zoomplate (b) LF Component (c) HF Component (d) Direction subband

Fig. 2. Zooneplate original image and NSCT decomposition results

There are two main steps in the decomposition process of NSCT. First, we use the stationary wavelet transform similar to pyramid algorithm to decompose, and then use non sub sampled directional filter banks to sample. Stationary wavelet transform realizes image multi-scale transformation. By using the same filter, we can get the next group of wavebands by using the same filter, and avoid the redesign of filter operation. The non sub sampled directional filter group cancels the down sampling operation of the original algorithm, so its main sampling is in the process of image decomposition. The up sampling algorithm is shown in Formula (3).

$$y[n] = \sum_{k \in mpp(k)} h[k]x[n - s[k]] \tag{3}$$

In formula, $y[n]$ for output, $h[k]$ is a given filter. $s[k]$ is a sample matrix. $x[n]$ is the waveband matrix. From the formula 3, we can see that the advantage of the NSCT algorithm is to achieve multi-scale and multi-directional decomposition without increasing the computational complexity of the algorithm. The decomposition process of. NSCT algorithm is shown in Fig. 3 [12].

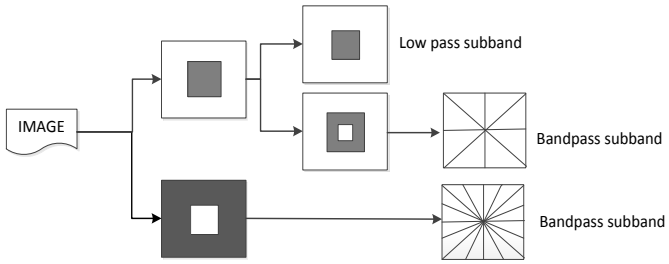

Fig. 3. Two layer NSCT decomposition flow chart

3.1 HOG operator

The first level high frequency components decomposed by NSCT contain the edge of the target, and the histogram of oriented gradient (HOG) operator is used for feature extraction. HOG algorithm can describe the edge features in a significant way. The specific steps are as follows: (1) normalize the high-frequency components after NSCT decomposition, normalization can reduce the influence of different background and illumination, and enhance the robustness of the algorithm. (2) Calculate every position in the image (x).The gradient values and directions in Y) are shown in formula 4 and formula 5.

$$G(x,y)=\sqrt{G_x(x,y)^2+G_y(x,y)^2} \tag{4}$$

$$a(x,y)=\tan^{-1}\left(\frac{G_y(x,y)}{G_x(x,y)}\right) \tag{5}$$

If the length and width of the high frequency component of NSCT is 128, the gradient direction is set to 8 directions, the size of the area (cell) is set to 8, and the normalization of 4 cell is achieved. The 8*4=32 dimension feature vector can be obtained, and the 15 windows of the X axis direction and the Y axis direction can be scanned, and finally the HOG characteristic dimension is 15*15*32=7200Victoria.

3.2 LBP operator

The low frequency component of NSCT contains many features such as texture and background. The Local Binary Pattern (LBP) Operator is used to extract the low frequency component eigenvectors, which can significantly describe texture features. As shown in formula (6) [13]

$$LBP(x_c,y_c)=\sum_{p-0}^{p-1}2^p s(i_p-i_c) \tag{6}$$

Image location (x_c,y_c). The pixel value is i_c, i_p represents the value of the surrounding pixels. S The threshold function is defined as:

$$s(x)=\begin{cases}1 & if \quad x\geq 0\\ 0 & else\end{cases} \tag{7}$$

If the length and width of the low frequency components decomposed by NSCT are all 128, then the LBP features are $(128/3)^2 = 1764$ Victoria [14].

3.3 PCA dimension reduction

Because the dimension of the feature vector calculated by LBP and HOG is 8964, the recognition and classification of the recognition model is huge. In this paper, principal component analysis (PCA) is used to reduce the dimension of the data [15]. The steps of PCA dimension reduction are as follows:

1) Using Jacobi method (Jacobi) to find out the eigenvalues and arrange them in order of magnitude;

2) Calculate the principal component contribution rate and the cumulative contribution rate;

3) Select the components with the cumulative contribution rate of 85% or more corresponding to the main components;

4) Construct a feature vector set composed of principal components for later target recognition.

$$R = \begin{bmatrix} r_{11} & r_{12} & \Lambda & r_{1p} \\ r_{21} & r_{22} & \Lambda & r_{2p} \\ \mathrm{M} & \mathrm{M} & & \mathrm{M} \\ r_{p1} & r_{p2} & \Lambda & r_{pp} \end{bmatrix}$$

$$r_{ij} = \frac{\sum_{k=1}^{n}(x_{ki} - \bar{x}_i)(x_{kj} - \bar{x}_j)}{\sqrt{\sum_{k=1}^{n}(x_{ki} - \bar{x}_i)^2 \sum_{k=1}^{n}(x_{kj} - \bar{x}_j)^2}} \tag{8}$$

Each element of the correlation matrix R is computed with the formula 8. $R_{ij,}$ (i, j = 1,2,...P) is the correlation coefficient of the original variable x_i and x_j, $R_{ij} = r_{ji}$.

4. Image Recognition based on PNN

In 1989, Dr. F. Specht first proposed the Probabilistic Neural Network (PNN). The main idea is to set the error classification and minimize the expected risk and separate the decision space in the multidimensional input space. The theoretical basis is the Bayes minimum risk criterion (Bayes decision theory). It is a feedforward neural network developed by the radial basis function model, which is different from the traditional radial basis function. PNN is an artificial neural network based on statistical principle. According to the non parametric estimation of probability density, Bayes decision is made to get the classification results. Compared with the traditional feedforward neural network, it has a fast training speed in pattern classification, and can guarantee the optimal solution under the

Bayesian criterion, allowing the training samples to be increased or reduced without the need for long time training. As shown in Fig. 4, a PNN network structure model is presented [16]. And a PNN program flow are showed in the Fig. 5.

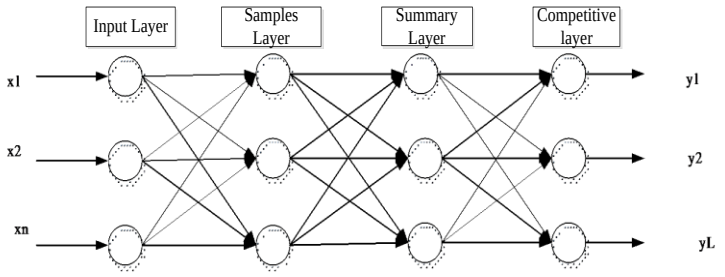

Fig. 4. PNN network model

As the distribution unit, the input vector is directly transferred to the sample layer. The number of nodes in the sample layer is determined by the product of the input sample and the class to be matched. The sample layer is weighted by the input from the input node, and then activated by an activation function. Then we pass it to the summation layer. Here the activation function uses the Gauss function, and the output showed as (9).

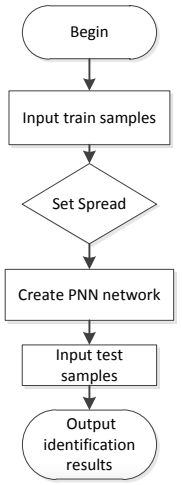

Fig. 5. PNN program flow chart

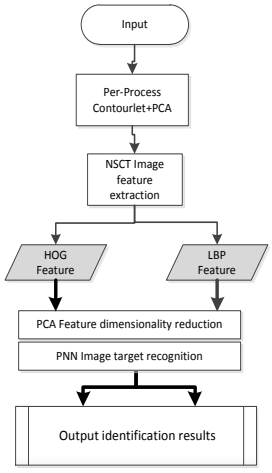

Fig. 6. Algorithm flow chart of this paper

$$\theta_i = \exp(-\sum(||x - c_i||^2 / 2\sigma_i^2)) \tag{9}$$

Among them, c_i For the radial basis function center, σ_i The formula 8 is used to calculate the similarity between the unknown mode and the standard mode for the switch parameter of the I component.[17]

The summation layer is connected to the class pattern element. p(x) According to the Parzen method, the probability of each type is estimated [18].

$$P(X \mid C_i) = \frac{1}{(2\prod)^{m/2}\sigma^m}\frac{1}{n}\sum_{i=1}^{n}\exp[-\frac{(X-X_i)^T(X-X_L)}{2\sigma^2}] \quad (10)$$

C_i category, X identifies samples. X_i For the pattern samples (weights) of category, i\m is vector dimension, σ for smoothing parameters, n is the number of pattern samples for class I.

The number of nodes in the decision level is equal to the number of classes to be matched. According to the probability of input, the Bayes classification rules are used to select the categories with the minimum risk. The decision method is expressed in the 10 formula [19].

$$P(X \mid C_i)P(C_i) > P(X / C_j P(C_j)) \quad (11)$$

When programming in MATLAB, it is necessary to select the smoothing factor spread of the appropriate size. The value is too large, the density estimation is smoother but the details are missing seriously. The value is too small, and the density estimation will show more spikes. The spread = 50 used in this paper will be tested.

5. Experiment and Discussion

The basic steps of SAR image recognition based on NSCT and PNN are three steps. (1) decomposing the source image by NSCT algorithm, acquiring multi-scale features, preserving the low-frequency components and the first high frequency components of the image; (2) extracting the hog features from the first stage high frequency components and extracting the LBP features from the low frequency components; (3) reducing the dimensions of the high-dimensional features obtained in step 2; (4) the feature vector after dimension reduction is used as the PNN input for network training. Finally, the experimental network is tested and the algorithm flow is shown in Fig. 6.

5.1 Data set

In this paper, MSTAR data collection standard operating conditions (SOC) acquisition conditions. The target image resolution is 0.3 m × 0.3 m, and the pixel size is 128 × 128. Four classes of 2343 SAR image targets are taken as experimental analysis objects, and rocket launch vehicle 2S1, prevention and control unit ZSU-234, tanks T72, armored vehicles BRDM2, as shown in Fig. 7 for four classes of targets. Among them, the 17 degrees view sample is 1192. The sample with a lateral view of 30 degrees is 1151 (as shown in Table 2).

Table 2

Sample number of four types of SAR images

Target	2S1	T72	ZSU-234	BRDM2
17。	299	298	297	298
30。	288	288	288	287

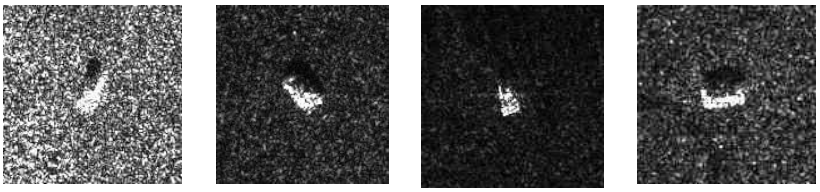

(a) 2S1 (b) BRDM2 (c) T72 (d) ZSU-234

Fig. 7. Target display of four kinds of SAR images

5.2 Experimental setup

The experimental platform of SAR image recognition is the PC of WINDOWS10 operating system. The configuration is 64 bit CPU of 2 GHz and AMD Ryzen5 2500, 8GB's RAM. Programming environment is MATLAB2019 version.

5.3 Result discussion

In order to verify the effectiveness of the proposed algorithm, four groups of algorithms were selected as the contrast experiments, namely Contourlet +SVM [20], NSCT (LBP) + PNN [21], NSCT (HOG) +PNN [22] and the NSCT+PCA+PNN algorithm proposed in this paper. The results of recognition are shown in Table 3.

Table 3

Experimental results comparison

	Test number	Correct number	Accuracy /%
Contourlet + PCA + PNN	1000	822	82.2
NSCT (LBP) + PNN	1000	805	80.5
NSCT (HOG)+ PNN	1000	814	81.4
Proposed	1000	904	90.4

The result of Table 3 shows that the recognition rate of Contourlet + SVM algorithm is 82.2%, the recognition rate of NSCT (LBP) + PNN algorithm is 80.5%, the recognition rate of NSCT (HOG) + PNN algorithm is 80.4%, the recognition rate of HOG feature and LEP feature of NSCT is 90.4%, which is 7.8 percentage points higher than that of the PNN algorithm. It shows that the NSCT algorithm is superior to the Contourlet algorithm in restraining noise and improving the recognition rate. Moreover, the recognition method proposed in this paper is 10 percentage points higher than the HOG feature alone and the LBP feature respectively, which shows that HOG and LBP features in NSCT play a role of feature fusion after PCA dimension reduction.

5.4 Robustness of the proposed algorithm

In order to further test the robustness of the algorithm, salt and pepper noise is added to the test set SAR image, and the signal to noise ratio(SNR) of the salt and pepper noise is 0.01,0.02,0.03,0.04 and 0.05 in sequence. Fig. 8 is the SAR image of the target under the five level noise. The 4 algorithms mentioned above are tested.

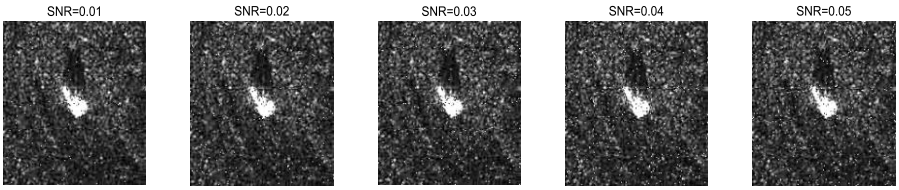

Fig. 8. The five level noise in the SAR image

Fig. 9 is a broken line diagram of the 4 methods for the recognition rate change under the influence of salt and pepper noise at five levels. From the broken line chart, it is shown that with the increase of SNR the recognition effect of Contourlet + PCA + PNN is the biggest, and other algorithms are reduced to varying degrees. Under the condition of five level noise, it only slightly declines by 3%, which proves the robustness and effectiveness of the proposed algorithm.

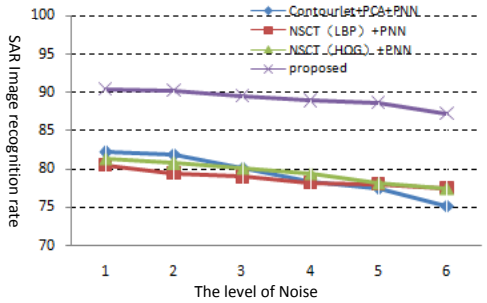

Fig. 9. Robustness test chart

6. Conclusions

In order to reduce the influence of noise and improve the recognition rate and robustness of SAR images. In this paper, a new generic method radar target recognition from radar images has been presented. It is based on SNCT and PCA+PNN. Affected by the speckle, the recognition rate of traditional SAR image recognition method is relatively low. Using NSCT to decompose the image, the high frequency and low frequency components can be obtained. Using hog operator to extract the features of edges and details in the high-frequency components. The LBP Operator is utilized to extract the features of low-frequency components such as texture and contour. Finally, PCA is used to reduce

dimension and classify the feature input into PNN network. Experiments verify the effectiveness of the proposed algorithm, and achieve 90.8% on the MSTAR database. At the same time, the robustness of the algorithm is tested. The results show that the algorithm is superior to single feature classification and principal component feature classification algorithm. This algorithm has better robustness. The disadvantage of the algorithm is that when PNN algorithm is used for multi classification, more input nodes lead to longer running time, and the next step is how to improve the efficiency of the algorithm.

Acknowledgments

Project supported by the science foundation of Inner Mongolia University of Technology (zz2018014)

R E F E R E N C E S

[1]. *A. Karine, A. Toumi, A. Khenchaf, M. Hassouni,* "Radar target recognition using salient keypoint descriptors and multitask sparse representation", in Remote Sens (Basel), **vol. 10**, no. 6, 2018, p. 843.

[2]. *A. Toumi, A. Khenchaf, B. Hoeltzener,* "A retrieval system from inverse synthetic aperture radar images", in application to radar target recognition, **vol. 12** no. 196, Sept. 2012, pp.73-96 .

[3]. *Z. Cui, S. Dang, Z. Cao, S. Wang, N. Liu,* "SAR target recognition in large scene images via region-based convolutional neural networks", in Remote Sens., **vol. 10**, no. 5, 2018, pp. 776-93.

[4]. *F. Gao, J. Y. Mei, J. P. Sun, J. Wang,* "Target detection and recognition in SAR imagery based on KFDA", in the Journal of Systems Engineering and Electronics, **vol. 26**, no. 4, 2015, pp. 720-731.

[5]. *Z. J. Liu, Y. F. Cao, X. C. Wang,* "SNTC algorithm for SAR image target recognition", in system engineering and electronic technology, **vol. 35**, no. 12, 2013, pp. 2489-2494.

[6]. *W. Wang, Y. D. Bi,* "SAR image recognition based on sparse manifold learning", in Acta electronica Sinica, **vol. 38**, no. 11, 2010, pp. 2540-2544.

[7]. *S. Song, B. Xu, J. Yang,* "SAR Target recognition via supervised discriminative dictionary learning and sparse representation of the SAR-HOG feature", in Remote Sens (Basel), **vol. 8**, no. 8, 2016, pp. 683.

[8]. *C. Szegedy, W. Liu, P. Sermanet, S. Reed*, "Going deeper with convolution", in Proceedings of IEEE conference on computer vision and pattern recognition (CVPR), Boston, M. A., USA, **vol. 8**, no. 10, June 2015, pp. 1-9.

[9]. *F. Wang, W. Sheng, X. Ma, H. Wang,* "Target automatic recognition based on ISAR image with wavelet transform and MBLBP", in Proceedings of the IEEE international symposium on signals, systems and electronics, Nanjing, China, 2010. pp. 1-4.

[10]. *G. Dong, G, Kuang,* "Classification on the monogenic scale space: application to target recognition in SAR image", in the IEEE Trans Image Process, **vol. 24**, no. 8, 2015, pp. 2527-2539

[11]. *J. P. P. Gomes, J. F. B. Brancalion, D. Fernandes,* "Automatic target recognition in synthetic aperture radar image using multiresolution analysis and classifiers combination", in Proceedings of the Radar conference, IEEE, 2008, pp. 1-5.

[12]. *H. Ruohong, Y. Ruliang,* "SAR target recognition based on MRF and Gabor wavelet feature extraction", in Proceedings of the IEEE international geoscience and remote sensing symposium, 2, IEEE, 2008, pp. II-907.

[13]. *M. Kang, K. Ji, X. Leng, Z. Lin,* "Contextual region-based convolutional neural network with multilayer fusion for SAR ship detection", in Remote Sens, **vol. 9,** no. 1, 2017, pp. 860-873.

[14]. *A. Krizhevsky, I. Sutskever,* GE. Hinton, "ImageNet classification with deep convolutional neural networks", in Proceedings of international conference on neural information processing systems (NIPS), lake Tahoe, Nevada, USA, **vol. 3**, no. 6, Dec. 2012, pp. 1097-105.

[15]. *A. Zaimbashi,* "An adaptive cell averaging-based CFAR detector for interfering targets and clutter-edge situations", in Digital Signal Processing, **vol. 16**, no. 8, 2014, pp. 86-92.

[16]. *C. Quintano, A. Fernández-Manso,* "Combination of Landsat and Sentinel-2 MSI data for initial assessing of burn severity", in the Appl. Earth Obs. Geoinf., **vol. 14**, no. 64, 2018, pp.221-225

[17]. *L. M. Kaplan,* "Improved SAR target detection via extended fractal features", in the Aerospace & Electronic Systems IEEE Transactions, **vol. 37,** no. 2, 2001, pp. 436-451.

[18]. *A. Mellor, S. Boukir,* "Exploring issues of training data imbalance and mislabelling on random forest performance for large area land cover classification using the ensemble margin", in ISPRS Journal of Photogrammetry and Remote Sensin, **vol. 44**, no. 5, 2015, pp. 91-98.

[19]. *C. Liu, C. H. Xie, J. Yang, Y. Y. Xiao, J. L. Bao,* "A method for coastal oil tank detection in polarimetric SAR images based on recognition of T-shaped harbor", in the Journal of Systems Engineering and Electronics, **vol. 29**, no. 3, 2018, pp. 499-509.

[20]. *A. Fischer, I. Christian,* "Training restricted Boltzmann machines: An introduction", in Pattern Recognition, **vol. 3**, no. 1, 2014, pp. 21-25.

[21]. *Y. Y. Wang, C. Wang, H. Zhang,* "Combining a single shot multibox detector with transfer learning for ship detection using sentinel-1 SAR images", in Remote Sensing Letters, **vol. 14**, no. 8, 2018, pp. 33-36

[22]. *K. Zhang, Z. Zhang, H. Wang, Z. Li, Q. Yu, W. Liu,* "Detection faces using inside cascaded contextual CNN", in Proceedings of IEEE international conference on computer vision 2017 (ICCV), Venice, Italy, 22-29 Oct. 2017, pp. 1-9.